ISSN 2616-5805 Vol. 7, Issue 1: 86-100, DOI: 10.25236/AJMS.2026.070112

First Braking Point Prediction Using Racing-Line Curvature in Formula 1 Hairpin Corners

Jiayin Song

Académie Ste-Cécile International School, 925 Cousineau Rd Windsor, Ontario, Canada

Abstract: *This study examines whether it is possible to use the curvature of a Formula 1 racer's driving line to help predict the first braking point in a hairpin corner. Telemetry data from the 2024 Japanese and Monaco Grand Prix qualifying sessions were collected using FastF1, and Suzuka Turn 11 and Monaco Turn 6 were chosen as two examples of hairpin corners. A fourth-degree parametric spline was used to interpolate coordinates of the racing line, while the curvature was calculated based on the first and second derivatives. A braking point was predicted as the first location in the selected corner region where curvature reached 20% of its maximum value. Prediction errors were computed across multiple drivers, and the results were compared with an empirical offset calibration method and a baseline comparison. After an abnormal outlier at Monaco was excluded, the original mean absolute errors (MAEs) were 40.48 m at Suzuka and 18.56 m at Monaco. Offset calibration reduced the MAEs to 11.15 m and 12.11 m, respectively. However, the mean-based baseline gave MAEs of 5.10 m at Suzuka and 4.75 m at Monaco. These results suggest that racing-line curvature alone is not enough to predict the accurate braking point in both corners. Future research could investigate whether including factors such as speed and braking behaviour improves prediction reliability.*

Keywords: *formula 1, racing-line curvature, braking-point prediction, spline interpolation, telemetry data*

1. Introduction

Formula 1 is a highly data-driven racing sport in which vehicle dynamics, driver behaviour, and track geometry all affect how a car's performance. Modern telemetry systems can record detailed information about a car's movement throughout a lap, including its position, speed, and braking input. This advanced technology makes it possible to analyze different aspects of driving behaviour mathematically.

Among all the aspects, braking is particularly important when entering a corner. The timing of braking has an impact on the car's corner entry speed and weight transfer between the front and rear tires. Braking too early may result in unnecessary time loss, and braking too late can cause tire lock-up or even run off the circuit. The location where braking begins, known as the braking point, can therefore be used to study a driver's cornering habits.

From a mathematical perspective, the shape of a racing line can be represented as a parametric curve using X and Y coordinates provided by telemetry data. Since the available telemetry data points are discrete, a spline interpolation is a useful way to connect those points smoothly. Curvature is also important in this study because of its close relation to the geometry of a corner. Physics also plays an indispensable role in researching Formula 1-related topics. A change in direction during cornering requires centripetal acceleration, while the friction circle describes the distribution of longitudinal and lateral forces acting on the car. These scientific concepts provide a theoretical basis for investigating whether there is a relationship between the geometry of a racing line and a driver's braking behaviour.

Previous studies have examined racing-line geometry and braking-point estimation from several different perspectives. Cheong & Chen (2025) employed cubic spline interpolation to model racing lines and calculate their curvature and the time taken for a race car to complete a corner[1]. Their work demonstrates how spline-based curvature can be incorporated into the mathematical analysis of an optimal racing line. However, the study mainly focuses on optimizing the racing line, rather than using curvature to identify a specific point within a corner, such as the first braking point. Peitzmeier, Mockenhaupt, and Reith (2023) developed a real-time braking-point estimation system for a Formula Student car[2]. Their approach involved the track section ahead and accounted for delays caused by

ISSN 2616-5805 Vol. 7, Issue 1: 86-100, DOI: 10.25236/AJMS.2026.070112

human reaction time. Although this work is directly related to the prediction of braking point, its approach does not directly address braking behaviour in Formula 1 due to different data sources. More recently, Bae, Nam, and Park (2026) analyzed Formula 1 racing lines using telemetry data from the 2024 season and introduced curvature-based metrics to describe the geometric difficulty of racing lines[3]. Their use of curvature primarily focuses on finding the mathematical and geometric properties of racing lines instead of predicting aspects of driving behaviour directly related to the driver.

These studies show that both curvature and braking-point estimation can be explored using mathematical models and telemetry data. Nevertheless, the direct relationship between the curvature of an actual Formula 1 driver's racing line and the first braking point after entering a corner has not yet been specifically examined. This leads to the main research question of this study: Can the curvature of a Formula 1 driver's racing line predict the first braking point after entering a hairpin corner?

To further investigate this question, a curvature-based mathematical model is developed using telemetry data from Formula 1 qualifying sessions. Hairpin corners are selected because their relatively small radius and great change in direction result in obvious geometric features of the racing line. FastF1 telemetry is used to reconstruct the drivers' racing lines and identify their actual braking points from brake input data. A fourth-degree spline is then incorporated to fit the recorded position values, and its curvature is calculated using derivatives. A constant curvature threshold ratio is used to predict the first braking point. The model is eventually evaluated across multiple drivers and hairpin corners by calculating the difference between the predicted and actual braking points.

The main contributions of this study include the use of real Formula 1 telemetry data to examine the relationship between racing-line geometry and braking behaviour, and the application of mathematical concepts such as spline interpolation and curvature to a real-world motorsport problem. In addition, an empirical offset calibration is applied to investigate whether systematic differences between predicted and actual braking points can be reduced. The model is also compared with a simple mean-based baseline to evaluate its predictive performance. By analyzing multiple drivers and hairpin corners, the study also provides a broader view of how this relationship may vary across different racing lines.

2. Theory

This section establishes the mathematical and physical foundations of the study. It introduces parametric curves, splines, curvature, centripetal acceleration, lateral force, and tire grip to describe the geometry and dynamics of a Formula 1 racing line. These concepts provide the theoretical foundation for the curvature-based prediction of the first braking point within the selected corner developed in the following sections.

2.1 Coordinate system

The drivers' racing lines are stored in a two-dimensional Cartesian coordinate system in the FastF1 dataset. Each telemetry point is represented by

$$(\mathrm{x}, \mathrm{y})$$

where x and y represent the horizontal and vertical coordinates of the car's position in units of $\frac{1}{10}$ m., respectively[4].

2.2 Parametric curve

Having discrete telemetry points, the next step is to connect these points and form a curve. Therefore, a two-dimensional parametric curve was used to represent the Formula 1 racing line as the car travels through a corner. Since the racing line cannot always be written as a function of $y=f(x)$, it is more appropriate to represent it parametrically as

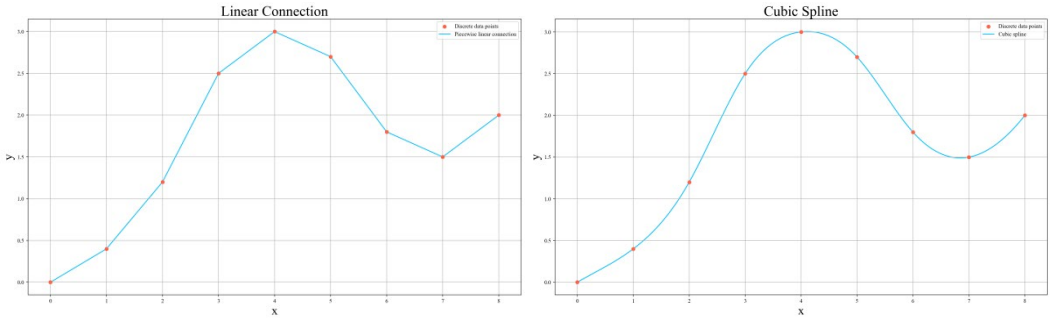
$$\boldsymbol{r}(u) = (x(u), y(u)) \tag{1}$$

where $x(u)$ and $y(u)$ represent the x and y position of the racing car, and u is a dimensionless parameter that describes the position along the fitted curve[5, p. 662].

ISSN 2616-5805 Vol. 7, Issue 1: 86-100, DOI: 10.25236/AJMS.2026.070112

2.3 Spline approximation

A spline is a piecewise polynomial function consisting of several polynomial sections. Compared with using a single high-degree polynomial interpolation, splines can approximate a set of data points using lower-degree polynomials defined over separate intervals. These polynomial segments are joined at specified points, called breakpoints, so that the resulting curve can maintain a smooth overall shape[6].



(a) Connected discrete points *(b) A smooth fitted cubic spline*

Figure 1. Comparison of line-segment and cubic spline representations

Figure 1(a) illustrates a linear piecewise connection of discrete points. Although it maximizes the goodness of fit of the function to each data point, fluctuations and cusps can be observed in the graph, which make the later calculations difficult. In contrast, Figure 1(b) introduces a cubic spline that passes through nearly all the points. The spline forms a smoother curve that is more amenable to subsequent mathematical analysis.

In this study, a fourth-degree spline was employed to approximate the general trend of discrete Formula 1 telemetry data.

2.4 Calculus on parametric curves

Given the parametric representation of the racing line from Equation (1), $\boldsymbol{r}(u) = (x(u), y(u))$, calculus operations can be applied to analyze its geometric properties. Suppose x and y are differentiable functions; the slope of the parametric curve can be written as:

$$\frac{dy}{du} = \frac{dy}{dx} \cdot \frac{dx}{du}$$

via the Chain Rule[5, p. 673].

Consequently, the first derivative of the curve with respect to the parameter u, which corresponds to the tangent vector, can therefore be expressed as:

$$\boldsymbol{r}'(u) = \left(\frac{dx}{du}, \frac{dy}{du}\right) \tag{2}$$

Given the first derivative, the second derivative $r''(u)$, which describes how the tangent vector changes with the parameter u, can be represented as:

$$\boldsymbol{r}''(u) = \left(\frac{d^2x}{du^2}, \frac{d^2y}{du^2}\right) \tag{3}$$

2.5 Continuity and differentiability

2.5.1 Continuity

A function $f(x)$ is said to be continuous at x=a if the following three conditions are satisfied:

1) $f(a)$ exists

2) $\lim_{x \to a^-} f(x) = \lim_{x \to a^+} f(x)$ (the limit as x approaches a exists)

ISSN 2616-5805 Vol. 7, Issue 1: 86-100, DOI: 10.25236/AJMS.2026.070112

3) $\lim_{x\to a} f(x) = f(a)$ (the limit equals the actual value)[5, p. 115]

Similarly, a spline is continuous if adjacent polynomial segments meet at their shared breakpoints without any jumps or gaps.

2.5.2 Differentiability

If the derivative of a function $f(x)$, written as $f'(a)$, exists at x=a, then the function is said to be differentiable at x=a[5, p. 144]. The derivative is defined as

$$f'(a) = \lim_{h\to 0} \frac{f(a+h) - f(a)}{h} \tag{4}$$

For a spline, differentiability indicates that adjacent segments not only meet at the junction point but also have the same tangent. For any two adjacent segments $f_1(x)$ and $f_2(x)$, this can be expressed as

$$f_1'(a) = f_2'(a)$$

which further means that there are no sharp corners at the junction.

2.5.3 C^n Continuity

C^n continuity describes the continuity of a function and its derivatives up to the nth derivative, where n is a non-negative integer representing the degree of smoothness or differentiability[7].

For instance, C^1 continuity requires both the function and its first derivative to be continuous, while C^0 continuity requires only the function itself to be continuous. In this study, a quartic spline was used to provide a higher degree of smoothness for the parametric racing line. According to the standard continuity properties of polynomial splines, a quartic spline can achieve C^3 continuity, meaning that the function and its first three derivatives are continuous. This ensures that the second derivative is not only continuous but also differentiable, which is beneficial for the subsequent curvature calculation and visualization.

2.6 Curvature

The curvature of a curve at a given point measures how quickly the curve changes direction at that point. Mathematically, curvature(κ) can be defined as

$$\kappa = \left|\frac{d\boldsymbol{T}}{ds}\right| \tag{5}$$

where T is the unit tangent vector and s is the arc length[5, p. 906].

For a parametric curve defined by $\boldsymbol{r}(u) = (x(u), y(u))$ from Equation (1), where $x'(u)^2 + y'(u)^2 > 0$, the curvature $\kappa(u)$ can be computed directly from the first and second derivatives with respect to the parameter u as follows:

$$\kappa(u) = \frac{|x'(u)y''(u) - y'(u)x''(u)|}{(x'(u)^2 + y'(u)^2)^{3/2}} \tag{6}$$

using the first derivative and second derivative in Equations (2) and (3).

Furthermore, curvature(κ) is also related to its radius of curvature(R):

$$\kappa = \frac{1}{R} \tag{7}$$

Therefore, a large curvature implies a sharp turn with a small radius of curvature, while a small curvature indicates a gentler one with a large radius of curvature.

2.7 Centripetal acceleration

Racing cars experience curved motion when passing through a corner, during which the direction of velocity continuously changes. Therefore, acceleration is generated in this process. This acceleration has a component directed toward the center of curvature and is known as centripetal acceleration. For motion along a curve, the magnitude of centripetal acceleration can be expressed as

ISSN 2616-5805 Vol. 7, Issue 1: 86-100, DOI: 10.25236/AJMS.2026.070112

$$a_c = \frac{v^2}{R} \tag{8}$$

where a_c is the centripetal acceleration, v is the velocity of the car, and R is the radius of curvature[8].

As mentioned in 2.6, curvature and the radius of curvature are reciprocal values of each other. Consequently, if replacing R with κ, Equation (8) can also be represented as

$$a_c = v^2\kappa \tag{9}$$

This relationship shows that a larger curvature requires greater centripetal acceleration at a given velocity.

2.8 Lateral force

According to Newton's Second Law, the acceleration of an object depends on the mass of the object and the amount of force applied. The mathematical definition is

$$F = m \cdot a$$

where m is the mass of the object and a is the acceleration[9].

The lateral force required for a racing car to navigate a curve can then be approximated by applying the centripetal acceleration from Equation (9):

$$F_{\text{lateral}} = mv^2\kappa \tag{10}$$

This equation indicates that the required lateral force increases if either the car's speed or the curvature of the racing line increases.

2.9 Tire grip and friction circle

The lateral force that a racing car can generate is limited by the grip between its tires and the track surface. The maximum force that a tire can withstand before losing its grip and beginning to slide is known as the adhesive limit, or stiction. Mathematically, the limit of the friction force can be expressed as

$$F_{friction} \leq \mu N \tag{11}$$

where μ is the coefficient of friction and N is the normal force acting on the tire. In a basic model that neglects aerodynamic force, the normal force can be approximated by the gravitational force,

$$N \approx mg \tag{12}$$

However, under the high-speed conditions encountered in Formula 1, the aerodynamic downforce increases the normal force acting on the tires, therefore increasing the maximum available friction force[10].

By combining Equations (11) and (12), the maximum friction force can therefore be written as

$$F_{friction_{max}} \approx \mu mg \tag{13}$$

However, lateral force is not the only force produced by tires in Formula 1. A racing car often needs to generate both lateral and longitudinal forces at the same time. Lateral force is required for cornering, while longitudinal force is associated with braking or acceleration. In order to visualize the relationship between these forces, the friction circle is introduced as a graphical representation[11].

ISSN 2616-5805 Vol. 7, Issue 1: 86-100, DOI: 10.25236/AJMS.2026.070112

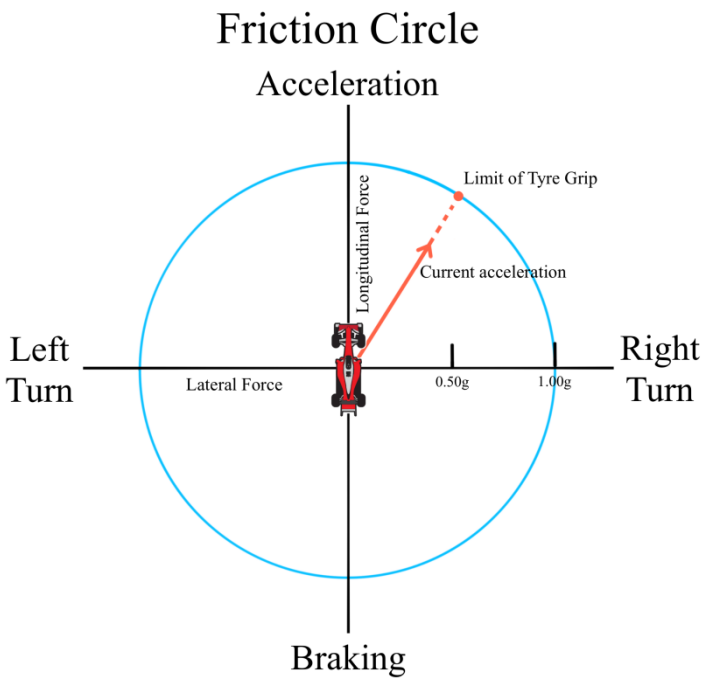


Figure 2. Friction Circle

Since the total force that tires can provide is limited by their grip, the lateral and longitudinal forces cannot reach their maximum values simultaneously. This relationship can be represented by:

$$F_x^2 + F_y^2 \leq (\mu F_z)^2 \tag{14}$$

where F_x and F_y are the longitudinal and lateral forces, respectively, μ is the coefficient of friction, and F_z is the normal force acting on the tire. From Equations (11) and (13), the maximum friction force can be approximated as

$$F_{friction_{max}} \approx \mu F_z.$$

Therefore, Equation (14) can also be written in terms of the maximum friction force:

$$F_{lateral}^2 + F_{longitudinal}^2 \leq F_{friction_{max}}^2 \tag{15}$$

This equation greatly illustrates the trade-off between lateral and longitudinal forces, such that when more tire grip is used for turning, less remains for braking or acceleration.

3. Data

3.1 Data source

The data used in this study were mainly obtained from FastF1, which is a python package for accessing and analyzing Formula 1 results, schedules, timing data and telemetry[12]. The package provides both general information about the circuit and detailed telemetry data that can be applied to reconstruct a driver's racing line and examine vehicle behaviour throughout a corner.

Since the first braking point after entering a hairpin corner was selected as the prediction target, the analysis used Turn 11 at Suzuka circuit (shown in Figure 3.b) and Turn 6 (Fairmont Hairpin) at Circuit de Monaco (shown in Figure 3.a) as two representative hairpin corner examples.

ISSN 2616-5805 Vol. 7, Issue 1: 86-100, DOI: 10.25236/AJMS.2026.070112



(a) *Suzuka Turn 11* (b) *Monaco Turn 6*

Figure 3. Real photographs of two hairpin corners

Source: (a) Sim Racing Setup [13]; (b) Formula 1 [14].

Among all the races, this study utilized data from the qualifying sessions of the 2024 Formula 1 season Grand Prix. Qualifying data was selected because drivers aim to achieve their fastest lap with the influence of random factors minimized. In other words, the data recorded from qualifying sessions provide a relatively unbiased measurement to examine braking behaviour and assess the true capabilities of cars and drivers.

3.2 Telemetry data

Telemetry data were extracted from FastF1 for each selected hairpin corner and driver. The main variables used in this study were the X-coordinate, Y-coordinate, Distance, Speed, and Brake. The X and Y-coordinates describe the position of the car on the circuit in $\frac{1}{10}$ m, while Distance represents the distance travelled along the lap since the first sample in meters. The Speed and Brake variables provide information about the vehicle state during the corner and are used to identify the actual braking point[4].

FastF1 circuit information was first used to determine the distance range of the selected hairpin corners. For each corner, the circuit information provides its X and Y coordinates, which approximate the position of the corner in a manually defined 2D Cartesian coordinate system, as well as the corner number, angle, and distance along the circuit. The "Distance" variable in the following tables represents the location of the marker as a distance from the start line instead of the starting point of this specific corner. Telemetry points within this range were then extracted for further analysis.

Table 1. Circuit information of Suzuka Turn 11

X	Y	Number	Angle	Distance
-5964.645828	1876.742727	11	-126.423013	2890.475124

Table 2. Circuit information of Monaco Turn 6

X	Y	Number	Angle	Distance
-797.246765	-1127.089111	6	-85.862753	1220.094025

The distance range of each corner in this study was determined based on the distance provided by the circuit information. As shown in Table 1 & 2, the distances of Turn 11 at Suzuka Circuit and Turn 6 at the Circuit de Monaco are 2890.475124 m and 1220.094025 m, respectively. Accordingly, a range from 2770 m to 2980 m was selected for Turn 11, while a range from 1165 m to 1250 m was chosen for Turn 6. Accordingly, a range from 2770 m to 2980 m was selected for Turn 11, while a range from 1165 m to 1250 m was selected for Turn 6.

For each driver, the fastest qualifying lap was selected to obtain the corresponding telemetry data. The actual first braking point after entering the hairpin corner was identified from the "Brake" variable. It was defined as the first recorded telemetry point at which the Brake status changed from False to True after the car entered the selected corner region. This point was used as the actual braking point for evaluating the prediction model.

Table 3. Reference braking point of Suzuka Turn 11

Index	Distance (m)	Speed (km/h)	Brake	X (0.1m)	Y (0.1m)
319	2778.057140	253.950003	False	-6046.000000	684.000000
320	2785.858333	248.000000	True	-6023.414643	743.810580

ISSN 2616-5805 Vol. 7, Issue 1: 86-100, DOI: 10.25236/AJMS.2026.070112

Table 4. Reference braking point of Monaco Turn 6

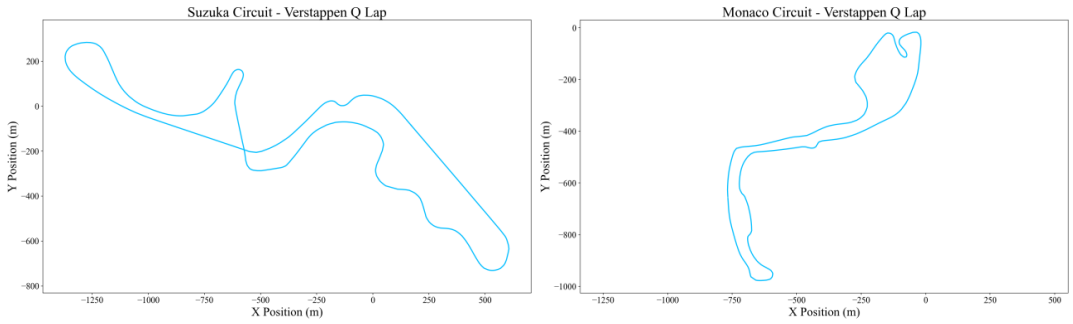
Index	Distance (m)	Speed (km/h)	Brake	X (0.1m)	Y (0.1m)
177	1166.954444	140.000000	False	-1059.128434	-883.481899
178	1177.244722	155.000000	True	-1002.000000	-958.904691

In Table 4, it is counterintuitive that the speed increases although the brake input changes from False to True. This occurs because the braking force does not necessarily reach its maximum value immediately when the brake is first applied. The net longitudinal force acting on the car may still be positive because the braking force is not yet large enough to overcome other longitudinal forces. As a result, the vehicle may continue to accelerate for a short period of time after braking input begins. The point at 1177.244722 m can still serve as the first actual braking point in this study.

4. Result

4.1 Racing line and speed profile

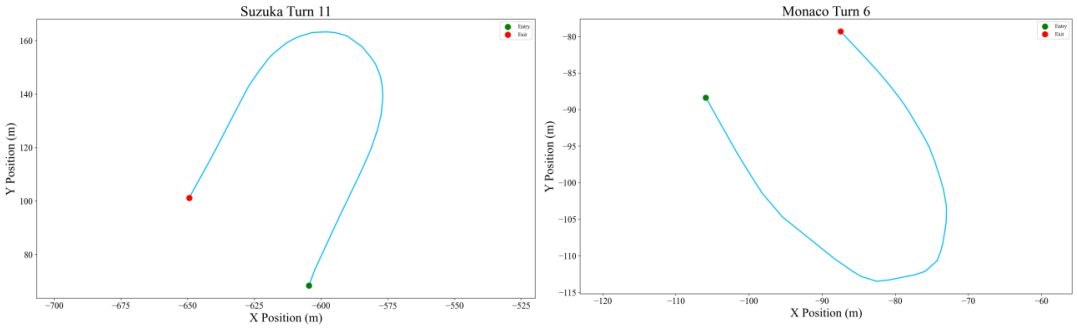
The prediction model was first demonstrated using Verstappen's fastest qualifying laps in the 2024 Japanese and Monaco Grands Prix as examples. Because this study selected Suzuka Turn 11 and Monaco Turn 6 (Fairmont Hairpin), we plotted the racing line for the full lap through each corner using X and Y coordinates from telemetry data imported from FastF1. Section 3.1 explains that the units for both X and Y positions in FastF1 are $\frac{1}{10}$ m. Therefore, the values on both axes were divided by 10 in the graph so that the units can always be expressed in meters.



(a) *Suzuka Circuit* (b) *Circuit de Monaco*

Figure 4. Verstappen's racing lines during his fastest qualifying laps at Suzuka and Monaco

In order to analyze the selected corners more specifically, they were isolated based on the data points within the distance ranges determined in Section 3.2.

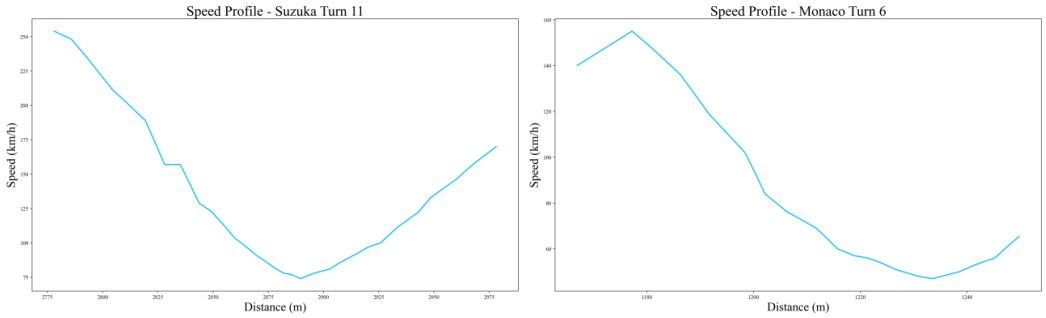


(a) *Suzuka Turn 11* (b) *Monaco Turn 6*

Figure 5. Telemetry-based racing lines of the selected hairpin corners

Since this study aims to predict the first braking point after entering a hairpin corner, the speed data were also examined over the same distance range. The speed profile was plotted against track distance to offer a clear observation of the vehicle's dynamic performance through the corner.

ISSN 2616-5805 Vol. 7, Issue 1: 86-100, DOI: 10.25236/AJMS.2026.070112

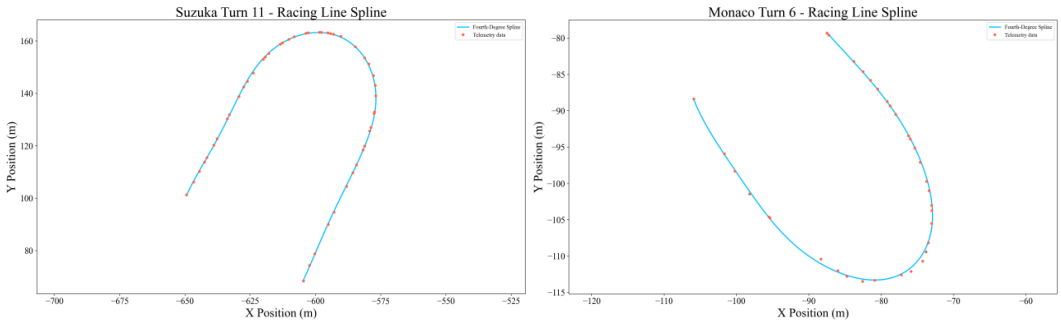


(a) *Suzuka Turn 11* (b) *Monaco Turn 6*

Figure 6. Speed profiles of the selected hairpin corners

4.2 Spline interpolation and curvature analysis

After extracting the telemetry data and visualizing the two corners, a fourth-degree spline was then fitted to the coordinates with a polynomial degree(k) of 4 and a smoothing factor(s) of 2. A smaller smoothing factor makes the spline fit to the original telemetry points more closely. Different smoothing factors were tested, and a value of 2 was eventually employed in the analysis to minimize the deviation between the simulated and real points. The spline curves of each corner were plotted together with the telemetry data to show the comparison(Figure 7).

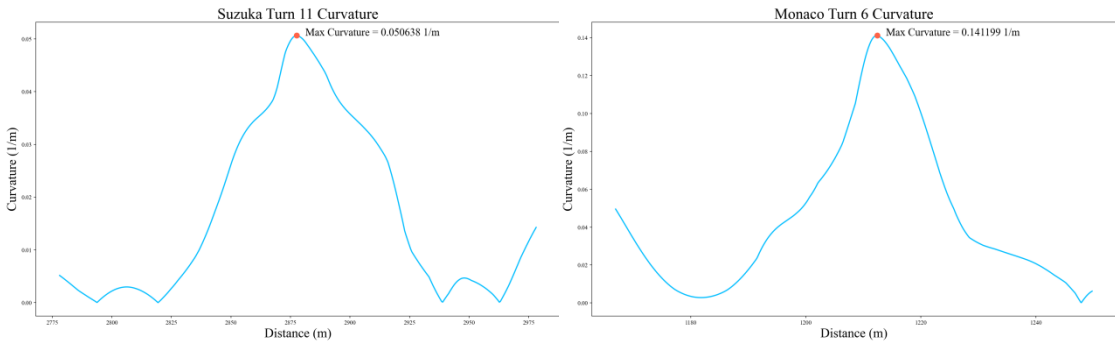


(a) *Suzuka Turn 11* (b) *Monaco Turn 6*

Figure 7. Fourth-degree spline fits of the selected hairpin corners

The fitted spline was then evaluated at 500 evenly spaced values of the parameter u between 0 and 1. The corresponding $x(u)$ and $y(u)$ values were obtained to represent the smooth racing line curve.

Curvature analysis is one of the most crucial parts of the prediction model. The first and second derivatives of each $x(u)$ and $y(u)$ were calculated and then plugged into the curvature formula, which is expressed in Equation (6) in Section 2.6. However, the result was still a relation between curvature and parametric u instead of recorded values of the circuit. In order to solve this issue, the spline parameter u was converted back to distance using linear interpolation based on the original u-distance data. In this way, the curvature at each of the 500 discrete points can be plotted versus track distance, resulting in curvature graphs of the two selected corners.



(a) *Suzuka Turn 11* (b) *Monaco Turn 6*

Figure 8. Curvature profiles and maximum curvature points of the selected hairpin corners

ISSN 2616-5805 Vol. 7, Issue 1: 86-100, DOI: 10.25236/AJMS.2026.070112

As stated in Equation (7), curvature and radius of curvature should present opposite trends. Because the radius of curvature(R) decreases sharply while entering the corner, reaches its minimum value at the apex, and then increases as the car begins to exit the corner, the curvature graphs should show a trend of first increasing and then declining. Figure 8 clearly illustrates this pattern, which is consistent with the geometric characteristic of hairpin corners.

Small fluctuations can also be observed in both curvature curves. These may be caused by slight variances in the recorded X and Y coordinates. Since curvature is calculated using the first and second derivatives of the spline, the graph can be sensitive to tiny changes in the fitted curve. Although the fitted spline was already utilized to make the original telemetry points smooth and reduce these fluctuations, those fluctuations cannot be eliminated.

4.3 Braking point prediction

The actual braking point has already been determined from the brake input data presented in Table 3 & 4 in Section 3.2. In order to find the difference between the actual and predicted braking points, the predicted braking point was calculated using the developed model. As shown in Figure 8 in Section 4.2, the maximum curvature values of Suzuka Turn 11 and Monaco Turn 6 are 0.050638 m^{-1} and 0.141199 m^{-1}, respectively. However, this point cannot be considered the first braking point directly because it generally occurs near the corner apex. Therefore, a threshold-based approach was introduced. In this study, a threshold ratio of 20% was applied, which means the distance of the predicted braking point is where the curvature first reaches or exceeds 20% of the maximum curvature within the distance range. Mathematically, it can be defined as

$$D_{\text{predicted}} = \text{first } D \text{ such that } \kappa(D) \geq 0.20\kappa_{\max}$$

Given that both predicted and actual braking points were established, the deviation of the prediction was represented by the absolute difference between them.

$$\text{Difference} = \left|D_{\text{predicted}} - D_{\text{actual}}\right| \tag{16}$$

Using Verstappen's example, the results of the two corners can be shown as

Table 5. Comparison of actual and predicted braking points and their differences for Verstappen at Suzuka Turn 11 and Monaco Turn 6.

Circuit	Driver	Actual Braking Point (m)	Predicted Braking Point (m)	Difference (m)
Suzuka	VER	2785.858	2836.818	50.960
Monaco	VER	1177.245	1166.954	10.290

4.4 Results across drivers

The same process was then applied to all drivers with sufficient telemetry data. Each driver's fastest qualifying lap from the 2024 Japanese and Monaco Grands Prix was used for the analysis, while the distance range, threshold ratio, and smoothing factor were kept the same across all the drivers. The actual braking point, predicted braking point, maximum curvature, curvature threshold (20% of maximum), and difference were calculated for each driver at the two corners and summarized in Tables 6 & 7.

Table 6. Actual and predicted braking points, maximum curvature, curvature thresholds, and differences for the 19 drivers at Suzuka Turn 11.

No.	Driver	Actual Braking Point (m)	Max Curvature (m^{-1})	Curvature Threshold (m^{-1})	Predicted Braking Point (m)	Difference (m)
1	VER	2785.858	0.050638	0.010128	2836.818	50.960
2	PER	2796.590	0.050839	0.010168	2833.948	37.358
3	NOR	2797.854	0.048473	0.009695	2828.680	30.826
4	ALO	2804.132	0.046910	0.009382	2842.779	38.647
5	PIA	2796.746	0.050465	0.010093	2846.764	50.018
6	HAM	2794.903	0.050168	0.010034	2835.929	41.026
7	LEC	2798.933	0.048817	0.009763	2840.760	41.827

ISSN 2616-5805 Vol. 7, Issue 1: 86-100, DOI: 10.25236/AJMS.2026.070112

No.	Driver	Actual Braking Point (m)	Max Curvature (m^{-1})	Curvature Threshold (m^{-1})	Predicted Braking Point (m)	Difference (m)
8	RUS	2795.769	0.047770	0.009554	2835.644	39.875
9	TSU	2803.968	0.049724	0.009945	2839.992	36.024
10	RIC	2796.468	0.049967	0.009993	2835.438	38.970
11	HUL	2779.777	0.048373	0.009675	2837.847	58.071
12	BOT	2794.481	0.047264	0.009453	2838.726	44.245
13	ALB	2793.509	0.050767	0.010153	2833.692	40.183
14	OCO	2789.736	0.049548	0.009910	2840.959	51.223
15	STR	2799.458	0.047425	0.009485	2779.192	20.267
16	GAS	2787.742	0.049169	0.009834	2841.508	53.766
17	MAG	2794.659	0.050403	0.010081	2839.939	45.280
18	SAR	2781.822	0.046979	0.009396	2780.280	1.542
19	ZHO	2794.781	0.051501	0.010300	2843.834	49.052

Table 7. Actual and predicted braking points, maximum curvature, curvature thresholds, and differences for the 19 drivers at Monaco Turn 6.

No.	Driver	Actual Braking Point (m)	Max Curvature (m^{-1})	Curvature Threshold (m^{-1})	Predicted Braking Point (m)	Difference (m)
1	LEC	1179.092	0.138436	0.027687	1202.301	23.209
2	PIA	1181.754	0.131220	0.026244	1196.679	14.926
3	NOR	1183.574	0.171643	0.034329	1207.480	23.906
4	VER	1177.245	0.141206	0.028241	1166.954	10.290
5	HAM	1173.509	0.150924	0.030185	1199.806	26.297
6	TSU	1181.076	0.159722	0.031944	1168.987	12.089
7	GAS	1178.256	0.136739	0.027348	1197.652	19.396
8	OCO	1187.144	3419.385905	683.877181	1191.760	4.616
9	RIC	1183.508	0.155684	0.031137	1198.311	14.803
10	STR	1180.349	0.152535	0.030507	1197.679	17.330
11	HUL	1171.182	0.153300	0.030660	1201.922	30.740
12	ALO	1179.651	0.158444	0.031689	1200.123	20.472
13	SAR	1172.275	0.157097	0.031419	1194.411	22.136
14	MAG	1173.349	0.126293	0.025259	1194.478	21.129
15	PER	1172.382	0.131186	0.026237	1194.663	22.281
16	BOT	1190.283	0.173685	0.034737	1166.779	23.504
17	ZHO	1173.576	0.138793	0.027759	1165.188	8.389

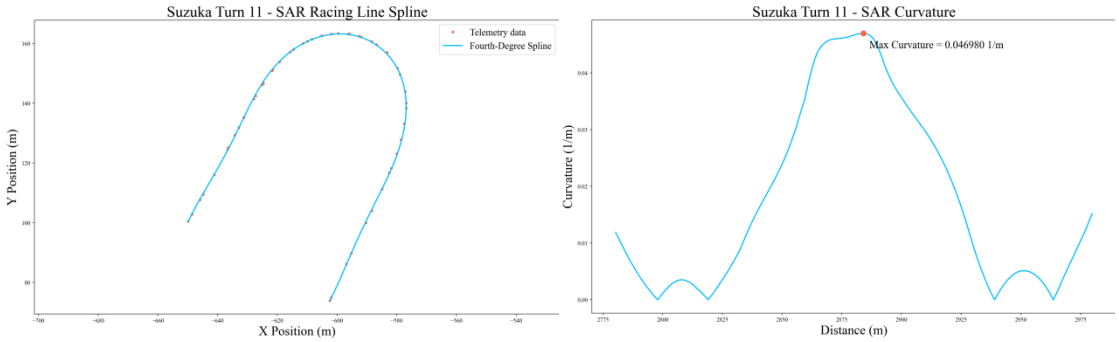
The results varied between drivers, suggesting that the geometric characteristics of each driver's racing line were different. However, most of them were within a similar range. The outcomes are discussed further in the next section using statistical analysis.

4.5 Outlier analysis

Examining the results in Tables 6 and 7, observations with abnormal results were identified. Logan Sargeant at Suzuka showed a relatively small prediction difference of 1.542 m, while Esteban Ocon at Monaco had an extremely large maximum curvature of 3419.385905 m^{-1} compared with the other drivers. Therefore, these two observations were initially identified as potential outliers. The original telemetry points, fourth-degree spline interpolations, curvature graphs, and the minimum denominator in the curvature calculation were examined to determine whether they were actual outliers that would affect the following statistical analysis.

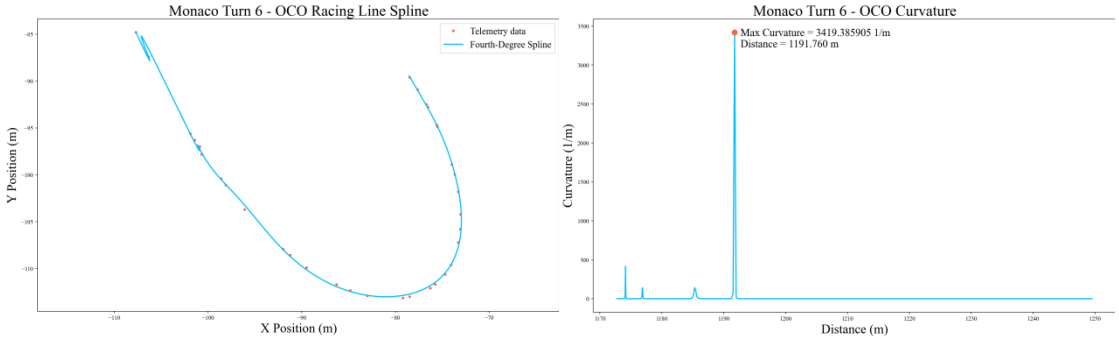
Figure 9 demonstrates Sargeant's spline curve of the racing line and the corresponding curvature graph at Suzuka Turn 11. The spline follows the original telemetry points closely, and the curvature plot shows a similar pattern to that described in Section 4.2 without an obvious abnormal spike. As shown in Figure 9 (b), the maximum curvature was 0.046980 m^{-1}, which was similar to the values of other drivers. This evidence suggests that although Sargeant's prediction difference was unusually small at 1.542 m, there was no apparent abnormality in the spline fit or curvature calculation. Therefore, Sargeant's result should not be considered an outlier or excluded from the dataset.

ISSN 2616-5805 Vol. 7, Issue 1: 86-100, DOI: 10.25236/AJMS.2026.070112



(a) Fouth-degree spline curve *(b) Curvature graph*

Figure 9. Sargeant's racing-line spline and corresponding curvature at Suzuka Turn 11



(a) Fouth-degree spline curve *(b) Curvature graph*

Figure 10. Ocon's Racing-Line Spline and Corresponding Curvature at Monaco Turn 6

For Ocon, it is clear that there are abnormalities in both the spline fit and curvature plot in Figure 10. Unlike Sargeant's results, the fourth-degree spline turns back near the beginning of the racing-line segment, and the curvature graph also contains extremely sharp spikes, with the maximum curvature of 3419.385905 m^{-1} occurring at a distance of 1191.76 m. In order to examine what caused this unusually large value, the minimum denominator within the range of 1165 m to 1250 m was calculated.

Table 8. Minimum value of the curvature denominator and its corresponding distance

Quantity	Value
Minimum curvature denominator	$4.199278523202 \times 10^{-1}$
Distance at minimum denominator	1191.760 m

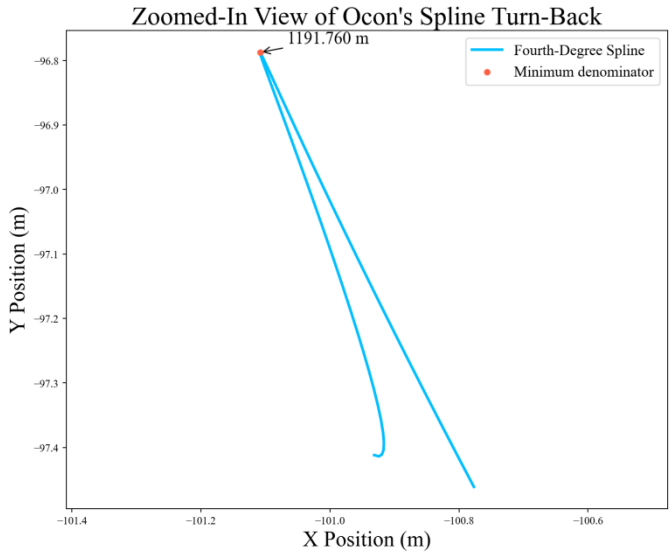


Figure 11. Zoomed-in view of Ocon's spline at Monaco Turn 6 near the minimum denominator point

As shown in Table 8, the minimum curvature denominator of Ocon's fitted spline was

ISSN 2616-5805 Vol. 7, Issue 1: 86-100, DOI: 10.25236/AJMS.2026.070112

approximately 4.1993×10^{-1}, occurring at 1191.76 m. The zoomed-in view in Figure 11 shows that the spline turns back near this same location. This causes the magnitude of the tangent vector, $\sqrt{x'^2 + y'^2}$, to become very small, resulting in a very small denominator in the curvature formula. Since the maximum curvature and minimum curvature denominator occurred at the same distance, the extremely large curvature was likely caused by this small denominator.

Based on the result table and visual analysis, Sargeant's result was retained, while Ocon's result was excluded from the dataset.

4.6 Statistical result and comparison between hairpin corners

4.6.1 Original prediction difference

Given the absolute difference for each driver, the mean value($\bar{D}$) and sample standard deviation(s) were calculated to describe the prediction differences for the two hairpin corners.

The mean difference can be mathematically defined as

$$\bar{D} = \frac{1}{n}\sum_{i=1}^{n} D_i \tag{17}$$

where D_i represents the difference for each driver and n is the number of drivers.

The sample standard deviation was calculated using the formula

$$s = \sqrt{\frac{\sum_{i=1}^{n}(D_i - \bar{D})^2)^2}{n-1}} \tag{18}$$

The resulting statistical values after removing the outliers identified in Section 4.5 for Suzuka Turn 11 and Monaco Turn 6 are

Table 9. Mean and standard deviation of the differences at Suzuka Turn 11 and Monaco Turn 6.

Circuit	Mean Difference ($\bar{D}$)	Standard Deviation (s)
Suzuka	40.482 m	12.842 m
Monaco	19.431 m	6.060 m

Since the distance ranges of the two hairpin corners are different, the absolute mean differences in meters cannot be compared directly. Instead, a relative difference can be calculated to represent a more applicable comparison.

$$\text{Relative Difference} = \frac{\bar{D}}{D_{\max} - D_{\min}} \times 100\% \tag{19}$$

where D_{max} is the upper bound and D_{min} is the lower bound of the predefined distance range of the corner. The relative differences were approximately 19.28% for Suzuka Turn 11 and 22.86% for Monaco Turn 6, and the two values were relatively similar.

4.6.2 Empirical offset calibration and baseline comparison

To improve the accuracy of the prediction, an empirical calibration was applied to the prediction model. First, the signed error (e_i) of each driver was calculated as the difference between the predicted braking point and the actual braking point:

$$e_i = D_{\text{predicted},i} - D_{\text{actual},i} \tag{20}$$

A positive value means that the model predicts a location later along the track than the recorded braking point, while a negative value means that the predicted braking point is earlier.

After that, a calibration offset b_i was obtained from the median signed error of the other drivers at the same corner:

$$b_i = \text{median}_{j \neq i}(e_j) \tag{21}$$

ISSN 2616-5805 Vol. 7, Issue 1: 86-100, DOI: 10.25236/AJMS.2026.070112

The driver i was excluded while calculating so that the driver being evaluated was not involved in the calibration of its own prediction.

The correction could be related to drivers' reaction time, since drivers may anticipate an upcoming corner and adjust their braking accordingly. However, these calculations do not establish that the calibration offset represents human reaction time. Therefore, it is referred to as an empirical offset correction in this study.

The corrected prediction can then be determined as

$$D_{\text{corrected},i} = D_{\text{predicted},i} - b_i \tag{22}$$

Finally, the mean absolute error (MAE) was computed as the mean of the absolute differences between the corrected braking points and the actual braking points. The MAEs for Suzuka Turn 11 and Monaco Turn 6 before and after calibration, excluding the outliers identified in Section 4.5, are shown in Table 10:

Table 10. Comparison of MAE before and after empirical offset calibration.

Hairpin Corner	Original MAE (m)	Corrected MAE (m)
Suzuka Turn 11	40.48	11.15
Monaco Turn 6	18.56	12.11

The results in Table 10 indicate that the calibration greatly reduced the prediction error at both corners.

For comparison, a simple baseline prediction was also tested. Each driver's braking point was predicted using the mean recorded braking point of the other drivers at the same corner. The calculated results were 5.10 m for Suzuka Turn 11 and 4.75 m for Monaco Turn 6.

Table 11. Comparison of MAEs among the original curvature model, empirical offset calibration, and mean-based baseline.

Method	Suzuka Turn 11 (m)	Monaco Turn 6 (m)
Original Curvature Model	40.48	18.56
Empirical Offset Calibration	11.15	12.11
Baseline Comparison	5.10	4.75

From Table 11, it is clear that although the corrected braking point substantially improved the prediction accuracy of the original model, the mean-based baseline comparison still performed better with lower MAEs. Therefore, the outcomes did not demonstrate that racing-line curvature provided additional predictive value beyond the simple mean-based approach.

5. Conclusion

This study used fourth-degree spline interpolation to calculate the curvature of Formula 1 racing lines and investigate whether it could predict the first braking point in hairpin corners. Overall, the original results showed that the predicted braking points were close to the actual braking points across the drivers, despite a remaining systematic offset. The relative differences for the two corners were also relatively close. These suggest that the curvature of a racing line contains useful information about where braking begins. However, the predicted and actual braking points were not identical for every driver, so only relying on curvature cannot determine the exact braking point. To improve the agreement between predicted and recorded braking onset, an empirical offset calibration was applied, which dramatically decreased the mean absolute error (MAE) at both Suzuka Turn 11 and Monaco Turn 6.

There are several limitations to this study. Firstly, only two hairpin corners from two qualifying sessions were analyzed, so the results may not represent other corners or circuits. Braking behaviour can also be influenced by factors such as vehicle speed, tire compound, and driver's personal driving style. Furthermore, the curvature threshold ratio of 20% and a smoothing factor of 2 were selected as modelling choices for this study and require further testing. The relationship described in Equation (9) motivates the use of curvature, but it does not mathematically determine that threshold. Consequently, these parameter choices may not work equally well for every corner. The accuracy of the curvature also depends on the quality of the telemetry data, since small changes in the X and Y coordinates can have an impact on the second derivatives used to calculate curvature.

ISSN 2616-5805 Vol. 7, Issue 1: 86-100, DOI: 10.25236/AJMS.2026.070112

Another limitation is that the current model may not be equally suitable for all types of corners and circuits. The model was tested on other types of corners, including s-curves, double-apex corners, and opening and tightening corners, but it did not perform as consistently as the hairpin corners. This issue may be caused by different geometric characteristics of these corners, which can affect the shape and curvature of the racing line.

Future research could therefore investigate how the model can be modified for different corner geometries. Different curvature threshold ratios, smoothing factors or prediction methods could be tested to check whether the model can be adapted to other types of corners. Moreover, a time-based model could be developed in which the predicted braking time is calculated as the time at the curvature threshold minus a lead time (tau). This lead time would need to be estimated and tested using each driver's telemetry. Considering additional variables that may affect the braking point could also help establish the model's applicability and improve the predictive accuracy.

References

[1] Cheong KZ, Chen CY. Minimization of Curvature with Cubic Spline Interpolation for Optimal Racing Line. Menemui Matematik (Discovering Mathematics). 2025; 47(1):91–104.

[2] Peitzmeier F, Mockenhaupt J, Reith D. Optimum Real Time Estimation and Interfacing of Braking Points for Racing Car. IEEE Transactions on Vehicular Technology. 2023; 72(2):1710–1719. Available from: https://doi.org/10.1109/TVT.2022.3211840

[3] Bae M, Nam T, Park Y. Curvature-Based Geometric Difficulty Analysis of Formula 1 Racing Lines. Applied Sciences. 2026; 16(3):1596. Available from: https://doi.org/10.3390/app16031596

[4] FastF1. Telemetry. Available from: https://theoehrly-fast-f1.mintlify.app/core-concepts/telemetry [Accessed 9th September 2026].

[5] Stewart J, Clegg D, Watson S. Calculus: Early Transcendentals. 9th ed., Metric Version. Cengage Learning; 2020.

[6] SciPy Developers. Piecewise polynomials and splines. Available from: https://docs.scipy.org/doc/scipy/tutorial/interpolate/splines_and_polynomials.html [Accessed 9th September 2026].

[7] Aalto University. Differential and Integral Calculus. Available from: https://openlearning.aalto.fi/mod/page/view.php?id=10327 [Accessed 10th September 2026].

[8] OpenStax. College Physics 1e. 6.2: Centripetal Acceleration. Available from: https://phys.libretexts.org/Bookshelves/College_Physics/College_Physics_1e_(OpenStax)/06%3A_Uniform_Circular_Motion_and_Gravitation/6.02%3A_Centripetal_Acceleration [Accessed 12th September 2026].

[9] NASA Glenn Research Center. Newton's Laws of Motion. Available from: https://www1.grc.nasa.gov/beginners-guide-to-aeronautics/newtons-laws-of-motion/ [Accessed 12th September 2026].

[10] Beckman B. The Physics of Racing, Part 2: Keeping Your Tyres Stuck to the Ground. Available from: http://autoxer.skiblack.com/phys_racing/phors02.htm [Accessed 13th September 2026].

[11] Beckman B. The Physics of Racing, Part 7: The Traction Budget. 1991. Available from: http://autoxer.skiblack.com/phys_racing/phors07.htm [Accessed 14th September 2026].

[12] Oehrly T, et al. FastF1. GitHub repository. Available from: https://github.com/theOehrly/Fast-F1 [Accessed 19th September 2026].

[13] Sim Racing Setup. ACC Suzuka Track Guide. Available from: https://simracingsetup.com/assetto-corsa/acc-suzuka-track-guide/ [Accessed 19th September 2026].

[14] Formula 1. Insight: What It Feels Like to Complete a High-Speed Lap Around Monaco. Available from: https://www.formula1.com/en/latest/article/insight-what-it-feels-like-to-complete-a-high-speed-lap-around-monacos.6EKiaTMOAG7MIse7YiKBii [Accessed 19th September 2026].